Self-Aligning and Self-Calibrating Capacitive Sensor System for Displacement Measurement in Inaccessible Industrial Environments

van de Ven, Oscar S.; Vogel, Johan G.; Xia, Sha; Spronck, Jo W.; Nihtianov, Stoyan

DOI
10.1109/TIM.2017.2764333

Publication date
2018

Document Version
Accepted author manuscript

Published in
IEEE Transactions on Instrumentation and Measurement

Accepted Author Manuscript. Link to published article (IEEE): https://doi.org/10.1109/TIM.2017.2764333

Self-Aligning and Self-Calibrating Capacitive Sensor System for Displacement Measurement in Inaccessible Industrial Environments

Oscar S. van de Ven*, Johan G. Vogel†, *Member, IEEE,* Sha Xia‡, Jo W. Spronck§, and Stoyan Nihtianov†, *Senior member, IEEE*

***Abstract*—High-precision positioning often requires high speed and high resolution displacement measurements in order to compensate for the small vibrations of critical components. The displacement sensor must be precise and stable over a long period of time to avoid expensive recalibration. This requires tight mounting tolerances, which are especially difficult to meet in inaccessible environments. The proposed sensor system is based on a capacitive sensor and consists of three subsystems: a mechanical 'zoom-in' system that performs self-alignment of the capacitive sensor electrode in order to reduce the mounting tolerances of the sensor; a real time capacitance-to-digital converter that employs an internal reference and electrical zoom-in technique to effectively reduce the dynamic range of the measured capacitance, thus improving the power efficiency; and a self-calibration circuit that periodically calibrates the internal references to eliminate their drift. In previous publications the three subsystems have been introduced. This paper shows how the different subsystems can be integrated to achieve optimal performance and presents new repeatability and stability measurement results. The overall system demonstrates a displacement measurement resolution of 65 pm (in terms of capacitance 65 aF) for a measurement time of 20 μs. Furthermore, the thermal drift of the sensor is within 6 ppm/K, owing to the self-calibration circuit. In measurement mode, the system consumes less than 16 mW.**

***Keywords*—Capacitive sensor, self-alignment, inaccessible environments, thermal actuator, high-resolution capacitive sensor interface, thermal stability, self-calibration.**

I. Introduction

In NUMEROUS industrial applications, the relative position of machine parts needs to be measured and controlled accurately [1]–[3]. Different types of displacement sensors are available for this purpose, all having their own advantages and limitations regarding resolution, measurement range, stability and build-in volume [4], [5]. If the displacement range is limited, capacitive sensors and eddy-current sensors are very attractive choices owing to their small size and low power consumption. Eddy-current sensors are relatively insensitive to environmental conditions [6], but for applications that require a high resolution typically capacitive sensors are utilised [7], [8]. Examples of applications that use capacitive sensors include dimensional metrology [9] and lithography.

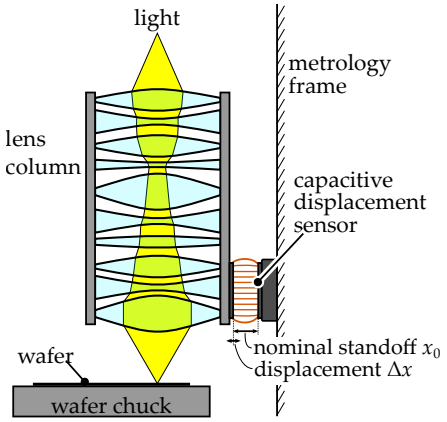

Fig. 1. Application example of a capacitive displacement sensor. In a a lithography machine, the wafer chuck must be dynamically aligned with the lens column. This requires a sub-nanometre precision displacement measurement of the lens column, leading to strict requirements regarding sensitivity, alignment and stability. Adapted from [10].

A lithography machine projects small details onto a wafer substrate that is carried by a wafer chuck (Fig. 1). To achieve sufficient imaging quality, the relative motion of the lens column and the wafer chuck must be well controlled. Any displacement of the lens column causes distortion of the image projected onto the wafer. To maintain imaging quality, the lens displacement with respect to the metrology frame must be measured with sub-nanometre precision [11], [12]. As the lens column is nearly stationary, only a small measurement range ($x_{\text{range}} < 1$ μm) is required.

Fig. 2 shows the sensor transfer characteristic $C(x) \propto 1/x$ of a capacitive displacement sensor, with x the distance between the capacitive electrodes. A lower distance leads to a higher sensitivity $S = \partial C/\partial x \propto 1/x^2$ [13]. Since the measured displacement is limited to a micrometer or less, and a high sensitivity is required, a low nominal distance (standoff) of only a few micrometers will be beneficial.

Operating at a low standoff requires the electrodes to

* Oscar S. van de Ven is with Ultimaker BV, Geldermalsen, The Netherlands. † Johan G. Vogel and Stoyan Nihtianov are with the Electronic Instrumentation Laboratory, Delft University of Technology, The Netherlands. § Sha Xia is with NXP semiconductors, Eindhoven, The Netherlands. Jo W. Spronck is with the group of Mechatronic System Design, Delft University of Technology, The Netherlands.

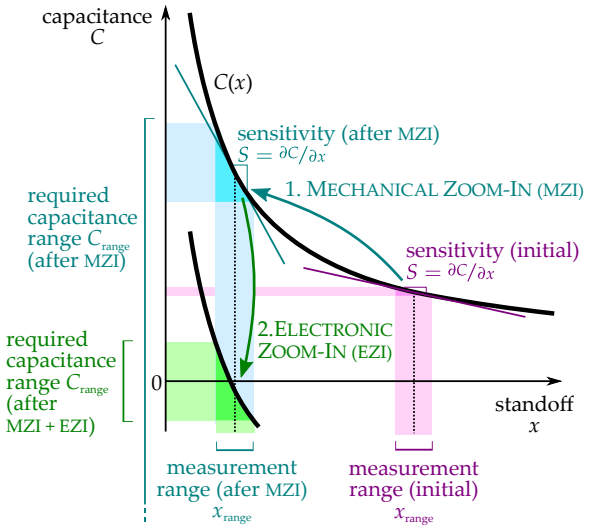

Fig. 2. Effect of Mechanical Zoom-In (MZI) and Electronic Zoom-In (EZI) on the sensor characteristic of a capacitive sensor. MZI increases the sensor's sensitivity, $S = \partial C/\partial x$. EZI virtually decreases the capacitance range C_{range} required by the capacitance-to-digital converter. Since the dynamic range is proportional to C_{range}/S, the MZI and the EZI together lead to an improvement in the dynamic range.

be brought into place and to be aligned accurately, which is not a trivial task. Many high-tech industrial machines, like lithography machines, are split into modules that are shipped separately and assembled at the customer's location. Since the modules might undergo significant shocks during transportation, the safe standoff must be over 100 µm. Thus, an alignment step is necessary during installation of the machine to bring the capacitive sensor closer to the target. At lower standoff, also tilt misalignment plays a larger role. Misalignment decreases the useful range [14].

The alignment of capacitive sensors is currently performed manually, a process that is time-consuming and costly, especially if the sensor is located at an inaccessible place in the machine. Therefore, a sensor with a 'mechanical zoom-in' functionality that autonomously brings it to the desired standoff and also aligns the capacitive probe during installation is of great interest.

Another practical issue concerns the cabling of the sensor. Conventional cabling between the capacitive probe and the readout electronics should be avoided, as it adds parasitic capacitance and interferences to the input of the electronic readout. Therefore, integration of the electronics into the probe is desired. However, the power dissipated by the electronics leads to self-heating of the probe, resulting in thermal drift of the readout electronics, the measurement electrode and the mechanical system, which deteriorates the system's stability. Therefore, the power efficiency of the electronics must be as high as possible.

The amount of power dissipated by the electronics is related to the dynamic range of the sensor, which for a given displacement resolution is proportional to C_{range}/S, with C_{range} as the capacitive measurement range and $S = \partial C/\partial x$ as the sensitivity. Fig. 2 illustrates that, given a certain displacement resolution, a smaller standoff leads to a lower dynamic range requirement and thus a lower power consumption.

Having decreased the standoff down to its minimum by mechanical zoom-in, the power can be further reduced by means of an 'electronic zoom-in' functionality (Fig. 2), which virtually decreases the capacitive range and thus the required dynamic range [15].

Finally, the precision of the capacitive sensor depends – amongst other factors – on the stability of the sensor's internal capacitive reference. Capacitive references typically drift over time, thus periodic recalibration is required.

To the best of our knowledge, there are no capacitive sensors available that have incorporated autonomous self-alignment functionality, i.e. mechanical zoom-in (1), in combination with electrical zoom-in (2) and capacitive reference self-calibration (3). In previous works we introduced these three functionalities [11], [16], [17]. In [18] a brief overview of the functionalities was presented, along with some early results.

This paper provides a complete and in-depth overview of the sensor system that combines the three functionalities, focusing on the collaboration between the subsystems, which is essential for obtaining high precision and high stability. Furthermore, extensive experimental results related to the alignment efficiency and stability in time and with room temperature are presented.

Section II provides an overview of the system architecture, introducing the subsystems, their interaction and the sensor's operation principle. Sections III, IV and V describe into depth the autonomous self-alignment, electronic zoom-in and the periodic recalibration functionality, respectively. Section VI shows the experimental results related to, amongst others, the noise and the stability of the sensor system.

II. Overview of the Proposed Sensor System

In this section, first the functions of the individual subsystems are introduced (A) and then the way the subsystems collaborate as a total system (B) is elaborated.

A. Subsystems and their function

Fig. 3 provides an overview of the capacitive sensor system with its three subsystems, i.e. a mechanical self-alignment system that performs mechanical zoom-in, a capacitance-to-digital converter that includes the electronic zoom-in functionality, and a high precision capacitance calibration circuit that minimises drift effects.

a) Mechanical self-alignment system (discussed in detail in Section III): Performs mechanical zoom-in to reduce the probe standoff distance from more than 100 µm down to ~10 µm, which is required during measurement. The self-alignment system addresses two contradictory requirements: (i) efficient positioning and alignment of the measurement electrode to the target electrode, and (ii) position stability

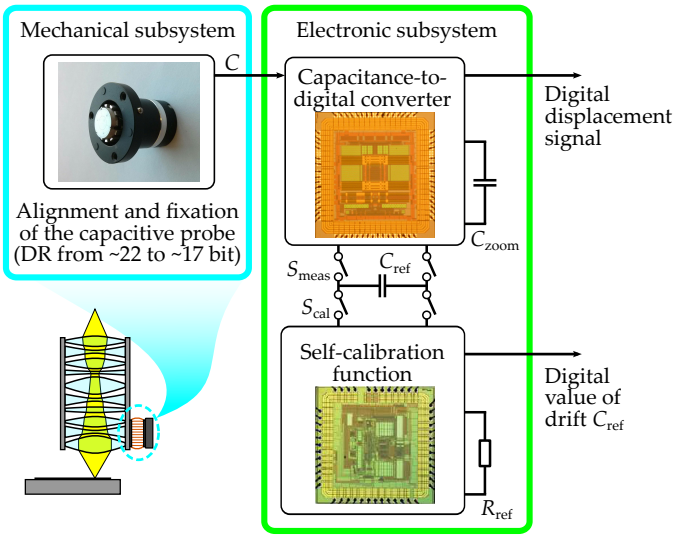

Fig. 3. Overview of the capacitive displacement sensor system, including three subsystems: the mechanical self-alignment system, the real-time capacitance-to-digital converter and the high-precision self-calibration function.

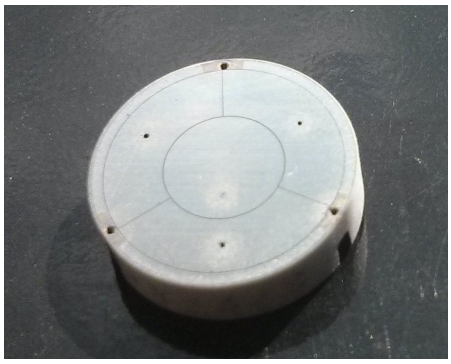

Fig. 4. Top view of the capacitive electrode. The electrode is segmented to be able to measure both position and the out-of-plane tilt angles.

of the measurement electrode during measurement. These contradictory requirements are both met by an alignment device that suspends the measurement electrode with friction contacts. These contacts can be manipulated on a submicrometre scale with an appropriate actuator and are able to provide the required stability in a passive way. As no power is dissipated in the actuator during measurement, parasitic thermal displacements and thermal loads to the electronics are avoided.

To be able to perform positioning and alignment, the system uses measurements of the capacitive electrode itself. For this purpose, the capacitive electrode is segmented (Figure 4). From the position measurements of the three ring sectors that surround the centre segment the position and the out-of-plane tilt angles are obtained.

b) Capacitance-to-digital converter (CDC) (discussed in detail in Section IV): Uses electronic zoom-in to reduce the effective capacitance measurement range, so that the capacitance readout electronics works more efficiently with respect to

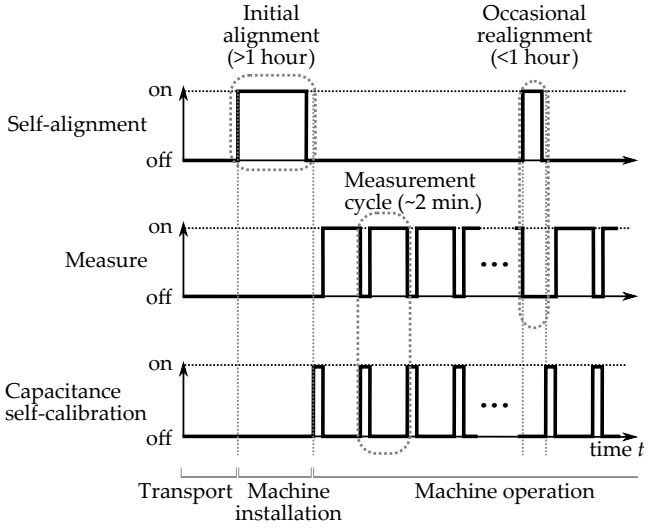

Fig. 5. The three operation modes of the capacitive sensor system (self-alignment, measurement and self-calibration) as a function of the phases of a machine's lifetime.

power consumption and conversion time. A "zoom-in" capacitance value that corresponds to the sensor capacitance at a nominal distance (~10 µm), is subtracted from the actual sensor capacitance value. This significantly reduces the dynamic range of the interface electronics, which improves its power efficiency and results in a reduced thermal load on the system.

c) Self-calibration function (discussed in detail in Section V): Reduces the sensitivity of the readout electronics to environmental conditions and self-heating, by periodic calibration.

The capacitors that are used as references for real-time measurement are sufficiently stable for short periods (a few minutes), but for longer time scales, thermal drift, stress and other factors limit the measurement precision. Periodically calibrating the capacitors by means of a much more stable combination of a resistive and a time reference improves long-term stability significantly. The periodic comparison of capacitance with resistance/time eliminates the need of continuous use of a stable reference, which would increase the total power consumption at high readout speeds. Also this would prevent straightforward implementation of the electronic zoom-in technique.

B. Collaboration between the subsystems

The sensor operates in one of three different modes, depending on whether the machine in which it is applied is transported, installed or operated. Fig. 5 shows the operation principles during the machine's lifetime. In the following sections, the collaboration between the different subsystems in each of the phases of the machine's lifetime, and the resulting subsystem requirements are elaborated on.

a) Transport: The machine in which the sensor system is incorporated must be transported from the manufacturing location to the operation location with the capacitive sensor already installed. As vibrations will be experienced during

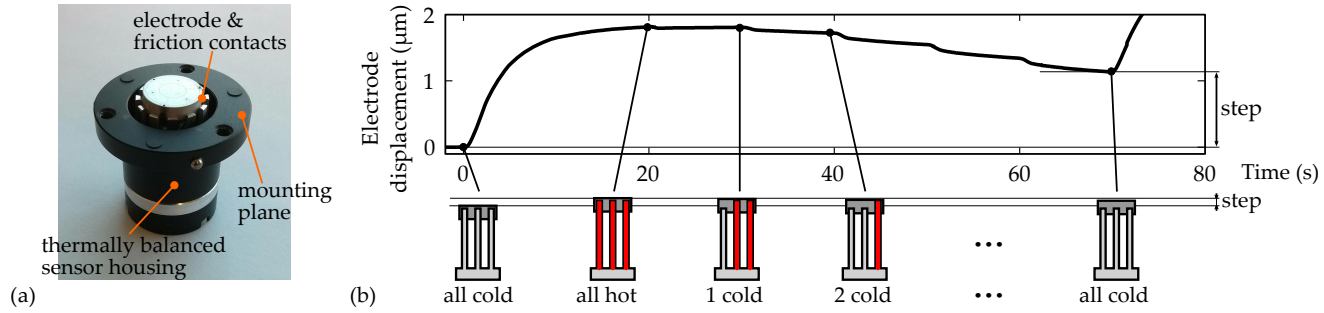

Fig. 6. (a) Industrial prototype of the Thermal Slider Actuator (TSA) with twelve fingers about 20 mm in length and an electrode disk with a diameter of 12 mm. (b) Schematic illustration of an upward thermal cycle of the TSA and the resulting electrode displacement step.

transport, the sensor is installed at a standoff distance larger than 100 µm.

b) Machine installation: During machine installation, the self-alignment functionality moves the measurement electrode until the distance to the target electrode is decreased to within 10 µm ± 1 µm and the two DoFs tilt alignment is within ±0.3 mrad. The alignment tolerances are several orders of magnitude below the precision requirements in the measurement phase, as in most applications no absolute but only relative precision is needed. The position and the two tilt angles of the electrode are obtained using the three circle sectors at the electrode. In order to do this, the position of each sector is obtained in a consecutive way, while all other segments are grounded. The position measurements of circle sectors are then decoupled to obtain the position and the two tilt angles.

The TSA dissipates during self-alignment up to ~10 W of power, depending on the number of fingers that is turned on. This leads to a self-heating of approximately 2 K to 3 K above ambient temperature and to thermal gradients in the TSA, which reduce the measurement precision of the system. Also, as the electrode is not yet aligned during this process, the position measurement has reduced precision. Although these effects do not lead to problems, due to the moderate precision requirements during machine installation, they could be decreased by adding smaller steps at the end of the alignment process.

Furthermore, the alignment phase is not time-critical, as the installation of a lithography machine takes days. Normally, a thermal actuation principle would be considered too slow and power-hungry for a precision positioning task. Given the application-specific boundary conditions, however, this is a viable and cost-effective solution.

c) Machine operation: In this phase the measurement precision, and thus the power dissipation as well, are critical. The self-alignment system in this phase should only provide position stability to the measurement electrode and therefore can be entirely passive. As the standoff distance is now small, the sensor sensitivity is high, leading to a measurement precision and resolution that are sufficient for sub-nanometre resolution measurement.

The most significant remaining uncertainty in the measurement then originates from the reference capacitors. These capacitances are on-chip and are as such not accurate or stable enough to attain sub-nanometre precision with the sensor system. As this uncertainty consists of low frequency variations mainly caused by the sensitivity to temperature, calibrating these quantities at the beginning of each individual measurement cycle eliminates this measurement error.

III. Mechanical Self-Alignment Mechanism

The mechanical self-alignment mechanism must 1) with micrometre precision actively move the measurement electrode in one translational and two tilt DoFs, and 2) afterwards hold the electrode passively with sub-nanometre stability. Many automatic positioning principles have been reported in the literature, including piezoelectric actuators [19], electrostatic comb drives [20] and thermal actuators [21]. Many of these concepts, however, provide stability in an active fashion, which requires an additional sensor and causes power dissipation during measurement.

To overcome these problems, the Thermal Slider Actuator (TSA) was designed [22]. The TSA achieves passive stability by exploiting the friction contacts between the fingers of the actuator and the disk-shaped measurement electrode. The fingers are thermally manipulated to produce movement.

A. Thermal Slider Actuator construction

Fig. 6a shows an industrial prototype of the TSA. The capacitive electrode is held by twelve fingers using friction contacts. The fingers are approximately 20 mm long and are connected monolithically to a base. The fingers are made of aluminium, as the high thermal expansion coefficient of aluminium is beneficial for the motion efficiency of the actuator. The fingers are actively heated by electrical resistors and are cooled passively.

The base of the fingers is mounted in a housing (Figure 7). This housing is made of aluminium, like the fingers, so that they have an equal thermal expansion coefficient. If the sensor's temperature changes uniformly, the fingers and housing expand with respect to the mounting plane of the sensor. However, since the contact points between the fingers and the capacitive electrode lie in the same plane as the mounting plane, they will not move. In this way, the thermal expansion coefficient of the fingers with respect to

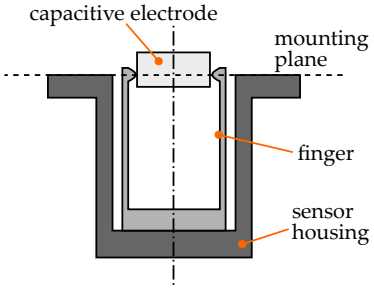

Fig. 7. Cross-section of the TSA. The fingers and sensor housing are made of the same material to balance the thermal expansion coefficient.

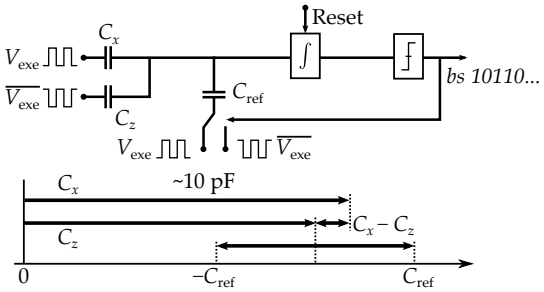

Fig. 8. Capacitance-to-digital converter based on a charge balancing ΣΔ modulator with the zoom-in technique.

the mounting reference plane is balanced, provided that there are no thermal gradients in the sensor. Still, the part of capacitive electrode that extends above the mounting plane causes thermal sensitivity, but this is only over a short distance (~1 mm) and can be reduced by choosing an electrode material that has a low thermal expansion coefficient.

B. TSA motion principle

Thermal cycles are used to displace the capacitive electrode in its translation and tilt DoFs [10], [18]. Fig. 6b illustrates how a thermal cycle generates a displacement step of the TSA's electrode. To move the electrode, all fingers are first heated, leading to thermal expansion and an upward displacement of the electrode. Then a single finger is cooled down, causing a shear force in the friction contact of the finger and opposite reaction forces distributed over all other fingers. Due to the friction behaviour of the contact, the cooling finger slides over the electrode surface, while the displacement of the other fingers contacts is close to zero, thus keeping the electrode in position. After all fingers have in this way cooled down, a net displacement of the electrode remains. As the thermal state is now identical to the initial state, the thermal cycle can be repeated to attain larger displacements. Furthermore, the thermal cycle can be adapted to yield downward and tilt motion.

The thermal cycles that are applied to the TSA must be selected such that they result in efficient displacement steps. Owing to the friction based working principle of the TSA, the repeatability of the thermal cycles is affected by variations in the thermal and frictional properties of the fingers. The motion, however, can be controlled in closed loop by using the position measurement of the capacitive electrode to select the most efficient thermal cycle. In this way, it was possible to reach the desired position within 0.7 µm and 50 µrad [10].

C. Stability

As any relative displacement of the electrode with respect to the machine forms a measurement error, the position stability during sensor operation should not be compromised by the actuator. The two main disturbances are temperature variation and displacement of the friction contact.

a) Thermal: The working principle of the TSA requires the materials of the actuator to have a relatively high thermal expansion coefficient. To minimise the thermal sensitivity of the sensor the housing of the TSA is purposely composed of equal length and material. Thus, the thermal expansion of the fingers due to external temperature variations is compensated by the thermal expansion of the housing.

b) Frictional: The friction contacts of the TSA make it possible to combine position stability with the capability to perform positioning and alignment. The fact that the friction contacts must be able to move potentially limits the position stability during measurement.

The classical stick-slip friction theory predicts that when the shear force in the friction contacts exceeds the friction force limit, a sudden displacement of the friction contact occurs. Instead of stick-slip, however, smooth contact creep was observed. The creep displacements, however, do not limit the position stability when thermal equilibrium is reached and the contact forces are small. Additionally, the strength of the stationary friction contacts increases over time, further improving the friction contact stability [10].

IV. Attofarad Resolution Capacitance-to-Digital Converter

In this work, the capacitance must be measured with very high resolution (~100 aF RMS, corresponding to ~100 pm in displacement, at a conversion time of 20 µs). Therefore, an interface circuit based on a charge balancing sigma-delta (ΣΔ) modulator is employed since it is a good candidate to achieve the required performance. However, as explained in Section III, the mechanical alignment can only help to reduce the mounting tolerance of the capacitive electrode to about 10 µm, while the long term measurement range of interest is not greater than 1 µm (corresponding to 1 pF). Furthermore, the displacement/capacitance variation in a measurement cycle between two calibrations is not expected to exceed ±25 nm/±25 fF. The consequence is that a large baseline (static) capacitance C_0 (~10 pF) is added to the short term maximum capacitance variation ΔC (±25 fF) to be measured. Therefore, a large amount of power is wasted to cover the unnecessarily large measurement range. In this case, the required dynamic range of the CDC is above 17 bits. The solution to this problem is to use the electrical zoom-in

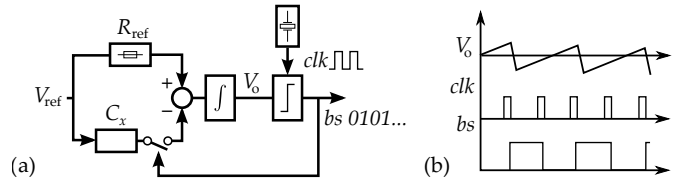

Fig. 9. (a) Block diagram of the proposed precision CDC based on a charge balancing ΣΔ modulator with a resistor/time reference; (b) Typical waveforms at critical nodes.

technique. A simplified implementation of the ΣΔ modulator with the zoom-in technique is illustrated in Fig. 8 [11].

V. Self-calibration function with external resistive reference

The chosen architecture in Section IV, based on the comparison of capacitances, provides a simplified practical realisation, high conversion speed and very good power efficiency [11]. However, as mentioned in Section II, the reference capacitors are expected to drift, both over time and along with temperature. A solution to this problem is to apply an additional built-in reference for periodic self-calibration that is much more precise and stable and to then calibrate at time intervals within which the drift of the capacitive references is acceptable. The calibration can be performed at suitable moments when no real-time measurement is required.

In this work, a high precision resistive reference is used with a drift of 2 ppm/K and an precision of 0.1 % [17], [23]. In order to compare capacitance with resistance, an additional reference component – frequency/time – needs to be included. Fortunately, the time reference can be very accurate and stable if a crystal oscillator is used. In this work, a quartz crystal oscillator with 0.2 ppm/K drift and precision greater than 0.01 % is used as the time reference [17], [23]. The comparison between C_x and the reference (t,R) is again based on the charge balancing technique with the ΣΔ modulator. The charge that is generated by the capacitance is balanced by the charge generated by the combined effect of resistance and frequency. Fig. 9a shows a simplified block diagram of the proposed self-calibration. The typical waveforms at critical nodes are shown in Fig. 9b.

The resistor reference is first converted into a current by a resistor-to-current converter (R-I converter) [17], [23]. Then, the combined precision current reference and crystal-stabilized time reference generate an equivalent charge reference. After the initial reset of the integrator, the modulator balances the charge supplied by the Capacitor Under Calibration (CUC or C_{cuc}) with the charge supplied by the equivalent charge reference. Using the same method as described in Section IV, the charge balancing operation can be expressed as:

$$N\frac{V_{ref}}{R_{ref}}T_{ref} = N_1 V_{ref} C_{cuc}, \tag{1}$$

where N_1 is the number of '1's in the output digital bitstream, and T_{ref} is the system clock period. The R-I converter employs the same reference voltage V_{ref} as the switched capacitor

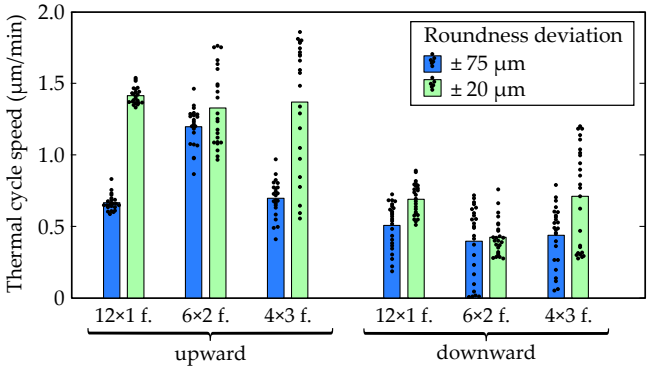

Fig. 10. Thermal cycle speed of the TSA for two roundness conditions, thee types of stepping sequences and up- and downward motion. Each point indicates the average speed during a single thermal cycle, the bar indicates the average speed of the thermal cycles.

feedback, so that the output is insensitive to the exact value and drift of V_{ref}, provided that the drift is much slower than the conversion time. The fact that this output is inversely proportional to C_{cuc} can be corrected in the digital domain, leading to a digital representation of C_{cuc} that only depends on stable resistive and time references:

$$C_{cuc} = \frac{N}{N_1}\frac{T_{ref}}{R_{ref}} = \frac{T_{ref}}{\mu R_{ref}}. \tag{2}$$

Ideally, if the conversion does not introduce an additional error, the precision of the measurement is purely dependent on the resistive and time references used. In practice, the electronics that compare the capacitance with the resistance introduce additional error which may deteriorate the measurement precision. Therefore, different circuit design techniques are applied to minimise the impact of the electronics such that the precision of the measurement satisfies the requirements [24]–[26].

VI. Experimental results

A. Mechanical self-alignment mechanism

a) Motion and repeatability: The TSA positions the measurement electrode in three DoFs by applying various thermal cycles to the fingers that clamp the electrode. The motion that results from a thermal cycle depends not only on the type of thermal cycle, but also on the initial temperature of the fingers and the mechanical conditions of the individual friction contacts. As the motion can be monitored using the capacitive electrodes themselves and only the final alignment must be highly precise, a precise open loop motion is not of highest importance. Stepping speed (i.e. the net displacement after a thermal cycle divided by its duration) is of interest, however, because it determines the time required to perform the alignment.

Fig. 10 shows the translational motion velocity of the thermal cycles under various conditions. A point shows the average speed of a single thermal cycle, the bars show the average speed of all similar thermal cycles. Due to the

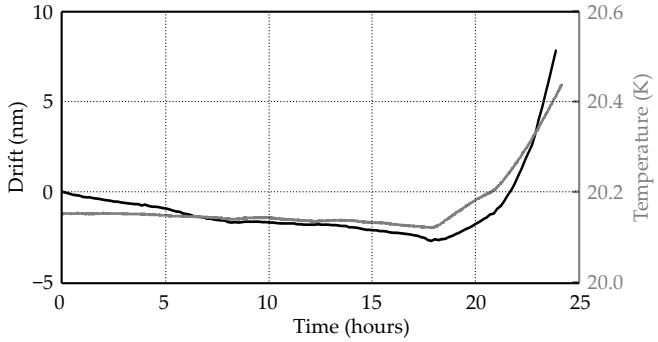

Fig. 11. Drift of the sensor electrode with respect to the mounting plane of the sensor (black) and temperature of the sensor's base (grey). The drift can to a large extent be explained by thermal drift. A thermal sensitivity of 24 nm/K can be fitted.

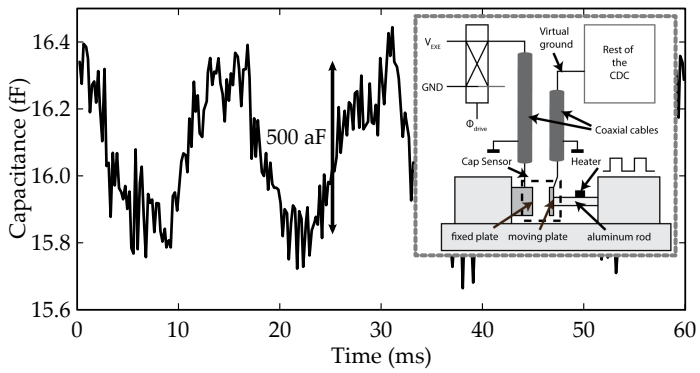

Fig. 12. Measurement result of the real-time CDC, the measured noise floor is 65 aF RMS. Insert: diagram of the measurement setup.

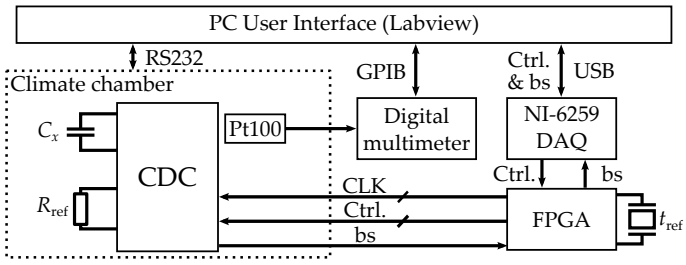

Fig. 13. Measurement setup for the self-calibration circuit for calibration of C_x using R_{ref}.

manufacturing process, the fingers of the TSA can have a deviation from their ideal radial position when no electrode is placed. These deviations lead to variation of the normal force of the friction contacts, influencing the motion of the thermal cycle. The initial roundness deviation after manufacturing was within $\pm$ 150 μm. This was not good enough to yield net motion. By mechanical adjustment of the straightness of the fingers, the roundness deviation was successively improved to within $\pm$ 75 μm and $\pm$ 20 μm. The figure shows that for the better roundness deviation of $\pm$ 20 μm, the thermal cycles always generate net motion and the speed of the thermal cycle improves.

Fig. 10 furthermore shows that the speed resulting from a thermal cycle in upward direction is higher than in downward direction. This difference can be largely explained by the asymmetry of the finger geometry: As the friction contact is offset from the bending axis of the finger, the friction force changes the normal force in the contacts. In the current design this leads to a higher friction force when a finger slides upward over the electrode then when the finger slides downward.

Three different thermal cycles for generating displacement were used, 12 steps×1 finger, 6 steps×2 fingers and 4 steps×3 fingers. The average speed of these cycles is comparable, but the 12×1 has highest repeatability. This can be explained by the fact that cycles with more steps are less sensitive to friction variations.

For positioning purposes also tilt cycles need to be used. Moreover, the cycles are also used in a more arbitrary order, leading to a lower repeatability of the resulting motion. It was however shown that despite these deviations, closed loop operation of the TSA can achieve sub-micrometre precision.

b) Stability and temperature sensitivity: After positioning, sub-nanometre stability is key to making the TSA applicable for electrode alignment. A setup was developed for measuring the position drift and the thermal stability of the TSA. The position of the electrode with respect to the mounting plane of the sensor was measured using a Fizeau interferometer and also the temperature of the sensor's base was monitored.

Fig. 11 shows the position drift of the capacitive electrode with respect to the mounting plane of the sensor during a 24 hours long experiment. The results suggest that the majority of the drift can be explained by thermal drift. A thermal sensitivity of 24 nm/K can be fitted. The remaining part of the drift is below 0.5 nanometre per hour, which is well below the short term (5 minutes) drift requirement of 100 pm.

B. Capacitance-to-digital converter

The prototype circuit of the real time CDC was fabricated in a standard 0.35 μm CMOS technology and consumes 15 mW from a 3.3 V power supply. A measurement result as well as the measurement setup are shown in Fig. 3. The sensor is connected to the interface via shielded coaxial cables, which adds ~10 pF parasitic capacitance to the input of the interface. The sensor target electrode is mechanically actuated by a shaker which shakes at 70 Hz, creating a small capacitance variation. The measured response of the sensor is shown in Fig. 12. It can be seen that the measurement noise floor is 65 aF RMS, which means that the equivalent displacement resolution is 65 pm RMS, if the standoff distance to the target is 10 μm. The measurement time for this interface is as short as 20 μs.

C. Self-calibration function

The self-calibration circuit (described in Section V) was also fabricated in standard 0.35 μm CMOS technology and consumes 760 μW power from a 3.3 V supply.

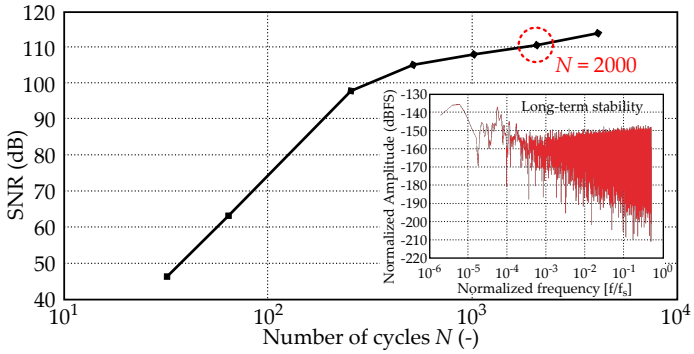

Fig. 14. Measurement resolution of the self-calibration circuit as a function of the number of operating cycles, N. Inset: noise spectrum of the self-calibration circuit from a twelve hours measurement.

To qualify the performance of the circuit, the measurement setup shown in Fig. 13 was built. The calibration circuit, as well as the precision resistive reference, were placed in a climate chamber that could be controlled remotely. The temperature of the system was measured with a Pt-100 sensor, which was in good thermal contact with the circuit chip.

First, the resolution of the calibration circuit was qualified by means of measuring the signal-to-noise ratio (SNR). Fig. 14 shows the measured SNR as a function of the operating cycles of the $\Sigma\Delta$ modulator [26]. As expected, a larger number of the operating cycles results in a better SNR. For our target application, the selected number of operating cycles is 2000 such that the circuit shows a noise floor of around 61 aF RMS, which is in line with that of the real time CDC. The total measurement time to achieve this level of resolution was around 10 ms.

The inset of Fig. 14 shows the result of the long-term stability measurement [17]. During this measurement, the environment in the climate chamber was maintained stably at $(25 \pm 0.01)\,^{\circ}\mathrm{C}$. The measurement was performed for 12 hours. A Fast Fourier Transform was calculated from the results. The noise spectrum can be seen in the inset of Fig. 14. The $1/f$ noise corner is at 200 µHz, ensuring that the drift of the circuit is extremely low. We suspect that the low-frequency noise observed can at least be partly attributed to small vibrations caused by the fan of the climate chamber.

To determine the thermal drift of the self-calibration circuit, the temperature of the climate chamber was swept from 20 °C to 70 °C [17]. For this measurement an on-chip capacitance was measured to avoid thermal gradients. In this test, ten chips were measured, all of which showed very similar, linear behaviour. The temperature drift for all the chips was around $+24$ ppm/K. However, these results are incorporated into the thermal drift of the measured on-chip poly-to-poly/PIP capacitor, which is specified to have a temperature coefficient of approximately $+30$ ppm/K [27]. Therefore, the thermal drift contributed by the CDC is around $+6$ ppm/°C across the entire temperature range of interest.

Table I. Performance summary of the proposed capacitive sensor system.

	During alignment	During operation
Alignment speed	> 0.5 µm/min	
Resolution		65 pm RMS
Measurement time		20 µs
Thermal drift (TSA)		24 nm/K
Thermal drift (readout)		6 ppm/K
Stability (TSA)		0.5 nm (1 hour)
Stability (readout)		100 pm (5 minutes)

VII. Conclusion

Precise real-time measurement of small displacements is challenging. In this work, the challenges of using capacitive sensors are identified and solved by the use of mechanical and electronic system improvements.

First, a mechanical self-alignment mechanism is introduced that effectively positions and aligns the capacitive sensor electrode after assembly. This eliminates the need for costly and time consuming manual alignment, especially in inaccessible environments. The self-alignment mechanism uses friction in combination with thermal actuation to move the electrode and is fully passive and powerless after alignment, thereby providing the required stability during measurement (100 pm over 5 minutes).

Second, the capacitance measurement is split in two phases: fast real-time power-efficient measurement using capacitive references and the zoom-in technique, and relatively slow periodic calibration of the capacitive references with a much more accurate and stable resistor/time reference. The performance of each subsystem has been experimentally verified, the main performance measures are summarised in Table I. The entire system combined can measure displacement with high resolution (65 pm RMS), high speed (20 µs/measurement), and high precision (6 ppm/K thermal drift and 100 pm stability for 5 minutes).

References

[1] D. S. Nyce, *Linear Position Sensors: Theory and Application*. John Wiley & Sons, 2004.

[2] G. C. Meijer, *Smart Sensor Systems*. Wiley Online Library, 2008.

[3] T. Castenmiller, F. Van de Mast, T. De Kort, C. Van de Vin, M. De Wit, R. Stegen, and S. Van Cleef, "Towards ultimate optical lithography with nxt: 1950i dual stage immersion platform," in *Proceedings of SPIE*, vol. 7640, 2010.

[4] Z. Chen, H. Pu, X. Liu, D. Peng, and Z. Yu, "A time-grating sensor for displacement measurement with long range and nanometer accuracy," *IEEE Transactions on Instrumentation and Measurement*, vol. 64, no. 11, pp. 3105 – 15, Nov. 2015.

[5] A. Fleming, "A review of nanometer resolution position sensors: operation and performance," *Sensors and Actuators A: Physical*, vol. 190, pp. 106 – 26, 2013.

[6] X. Ding, X. Chen, W. Ma, X. Chen, and N. Li, "A novel pqcr-l circuit for inductive sensing and its application in displacement detection," *IEEE Transactions on Instrumentation and Measurement*, vol. 65, no. 3, pp. 685 – 93, Mar. 2016.

[7] L. K. Baxter, *Capacitive Sensors: Design and Applications*. Wiley-IEEE Press, 1997.

[8] T. Addabbo, A. Fort, M. Mugnaini, S. Rocchi, and V. Vignoli, "A heuristic reliable model for guarded capacitive sensors to measure displacements," in *IEEE International Instrumentation and Measurement Technology Conference (I2MTC) Proceedings*, May 2015, pp. 1488 – 91.

[9] K. Bouderbala, H. Nouira, M. Girault, E. Videcoq, and J. A. Salgado, "Effects of thermal drifts on the calibration of capacitive displacement probes at the nanometer level of accuracy," *IEEE Transactions on Instrumentation and Measurement*, vol. 64, no. 11, pp. 3062 – 74, Nov. 2015.
[10] O. S. van de Ven, "Active positioning and passive fixation using friction in capacitive displacement measurement applications," Ph.D. dissertation, Delft University of Technology, Oct. 2016.
[11] S. Xia, J. P. van Schieveen, S. Nihtianov, and J. W. Spronck, "Concept evaluation of a high performance self-aligning capacitive displacement sensor," in *IEEE International Conference on Industrial Technology*, 2010, pp. 1575 – 80.
[12] S. Xia, K. Makinwa, and S. Nihtianov, "A capacitance-to-digital converter for displacement sensing with 17b resolution and 20 μs conversion time," in *2012 IEEE International Solid-State Circuits Conference*, Feb. 2012, pp. 198 – 200.
[13] S. Nihtianov, "Measuring in the subnanometer range: capacitive and eddy current nanodisplacement sensors," *IEEE Industrial Electronics Magazine*, vol. 8, no. 1, pp. 6 – 15, Mar. 2014.
[14] T. Hicks, P. Atherton, Y. Xu, and M. McConnell, *The Nanopositioning Book*. Queensgate Intstruments Ltd., Berkshire, UK, 1997.
[15] S. Xia and S. Nihtianov, "Power-efficient high-speed and high-resolution capacitive-sensor interface for subnanometer displacement measurements," *IEEE Transactions on Instrumentation and Measurement*, vol. 61, no. 5, pp. 1315 – 22, May 2012.
[16] J. P. van Schieveen, R. Yang, S. Nihtianov, and J. W. Spronck, "Performance optimization of a self-alignment system for capacitive sensors," in *Mechatronics (ICM), 2011 IEEE International Conference on*, Apr. 2011, pp. 648 – 53.
[17] R. Yang, M. A. P. Pertijs, S. Nihtianov, and P. Haak, "Capacitive sensor interface with precision references," in *IEEE International Conference on Industrial Technology (ICIT)*, Feb. 2014, pp. 358 – 90.
[18] O. S. van de Ven, R. Yang, S. Xia, J. P. van Schieveen, J. W. Spronck, R. H. Munnig Schmidt, and S. Nihtianov, *Autonomous self-aligning and self-calibrating capacitive sensor system*. Springer Berlin Heidelberg, 2012, pp. 10 – 7.
[19] L. Chassagne, S. Topcu, Y. Alayli, and P. Juncar, "Highly accurate positioning control method for piezoelectric actuators based on phase-shifting optoelectronics," *Measurement Science and Technology*, vol. 16, no. 9, p. 1771, 2005.
[20] C.-J. Kim, A. P. Pisano, R. S. Muller, and M. G. Lim, "Polysilicon microgripper," *Sensors and Actuators A: Physical*, vol. 33, no. 3, pp. 221 – 7, 1992.
[21] S. H. Lee, K.-C. Lee, S. S. Lee, and H.-S. Oh, "Fabrication of an electrothermally actuated electrostatic microgripper," in *TRANSDUCERS, Solid-State Sensors, Actuators and Microsystems, 12th International Conference on, 2003*, vol. 1, June 2003, pp. 552 – 5.
[22] J. P. v. Schieveen and J. W. Spronck, "Actuator and method for positioning an object," European Patent WO2 010 024 664 A1, 2009.
[23] *New generation of secondary standards hermetically sealed construction ultra-high precision z-foil technology resistors*, Vishay, 2010, available: www.vishayfoilresistors.com.
[24] M. A. Pertijs and J. Huijsing, *Precision Temperature Sensors in CMOS Technology*. Springer Science & Business Media, 2006.
[25] F. Witte, K. A. Makinwa, and J. Huijsing, *Dynamic Offset Compensated CMOS Amplifiers*. Springer Science & Business Media, 2008.
[26] R. Yang and S. Nihtianov, "Noise analysis and characterization of a charge-balancing-based capacitive sensor interface with a resistive reference," in *IEEE International Instrumentation and Measurement Technology Conference (I2MTC) Proceedings*, May 2014, pp. 1182 – 6.
[27] *C35B4C3 2P/4M 3.3V CMOS 4 metal, mixed signal, PIP, high-res poly, 5V periphery, product specification*, Austrian Microelectronics.